Intrinsic optical bistability for coated spheroidal particles

N. Kalyaniwalla and J. W. Haus
Department of Physics, Rensselaer Polytechnic Institute, Troy, New York 12180-3590

R. Inguva
Department of Physics and Astronomy, University of Wyoming, Laramie, Wyoming

M. H. Birnboim
Department of Mechanical Engineering, Aeronautical Engineering and Mechanics, Rensselaer Polytechnic Institute, Troy, New York 12180-3590

(Received 13 April 1990)

We present results on the nonlinear-optical response for a series of dielectric particles having nanometer sizes that are coated with a metallic shell. Using the freedom of changing particle shapes and coating thicknesses, we optimize the threshold intensity for intrinsic optical bistability. The metallic shell creates an enhanced local field in the nonlinear core. We report threshold intensities for silver-coated CdS as low as 12 W/cm^2.

I. INTRODUCTION

Engineered dielectric properties of heterogeneous materials for special applications has been a well-developed field for many years.[1] Recent research has discovered the possibility that enormous enhancements can be expected for nonlinear-optical response in composite materials containing metal particles.[2-6] Composite materials are made from small grains of semiconductor or metal particles that are dispersed in a glass matrix or a liquid. The particles are much smaller than a wavelength, but still large enough to be considered a bulk material, i.e., several nanometers in diameter.

There are two reasons to expect enhanced nonlinearities in these composite materials: (i) the particles have nanometer sizes and therefore the quantum confinement of the carriers can lead to increased binding and enhanced oscillator strengths,[7] and (ii) the local electric field inside the particles can be enhanced due to the difference between the dielectric properties of the particle and the host material. In metal particles the surface-plasmon resonance is used to obtain a strong enhancement of the local field.

In previous papers, we reported calculations predicting intrinsic optical bistability (IOB) in a composite material consisting of silver particles embedded in a silica matrix near the surface-plasmon resonance.[5,8] In these materials IOB occurs without a cavity because a resonance in the medium can be dynamically shifted by changing the intensity of the light in the medium. In our earlier paper,[8] we obtained a threshold intensity of 200 MW/cm^2 for silver particles. The threshold intensity can at best be reduced to about 20 MW/cm^2 by optimizing the shape of the silver particles. There is not much more that can be achieved with metals alone because the nonlinear response of these materials is weak. Furthermore, the absorption of electromagnetic waves is considerable so that the concentration of metal particles must be kept small.

The surface-plasmon resonance has also been proposed as a mechanism to increase the intrinsic nonlinearity of coated spheres.[9] We have studied these particles and optimized the coatings to produce enhancements of the nonlinear Kerr coefficient of several orders of magnitude. The coating offers another important degree of freedom in engineering the properties of the medium to find the largest nonlinear effects. For instance, the core of the particle can be chosen as a material which has an intrinsically large nonlinear response, such as a semiconductor nonlinearity due to an exciton resonance. The metal coating material is then chosen to enhance the field at the resonance frequency by using a surface-plasmon resonance effect.

Both the shape changes and the coating of the particles give us the freedom to optimize the threshold intensity for IOB in these new materials.[10] This is reported in this paper. The rest of the paper is organized as follows. In Sec. II we develop the theory treating single particles, the effective-medium theory and propagation effects. In Sec. III the results for several materials are reported and the optimization of these properties is discussed. We use experimental parameters for the semiconductors CuCl, CdS, and GaAs, for the silver and for the silica glass host material dielectric properties. Finally, in Sec. IV we present our conclusions.

II. THEORETICAL DEVELOPMENT

This section is divided into three parts: single-particle properties, effective-medium calculations, and propagation effects. In the first part, we present calculations for coated spheroidal particles. The second treats a medium consisting of a low concentration of these particles, which are oriented with respect to one another; the result is a dielectric function that treats the medium as homogeneous on the macroscopic scale, which is of course an effective medium. The third part uses the effective-

medium dielectric functions in Maxwell's equations and discusses the method of solution of the resulting equations.

A. Single particles

We consider spheroidal particle shapes, as illustrated in Fig. 1. Each small particle is taken to be composed of a spheroidal core of a given aspect ratio

$$r_c=(b_c/a_c)\ , \tag{1}$$

where b_c is the minor axis and a_c is the major axis. The particle shell is confocal with the core; the ratio of the minor to major axes is

$$r_s=(b_s/a_s)\ , \tag{2}$$

where b_s and a_s are the minor and major axes of the particle at the outer surface of the shell, respectively.

The spheroidal coordinates ξ_c and ξ_s define the outer surface of the core and the shell. When the core-shell interface is used the coordinate is ξ_c; ξ_s denotes the interface between the shell and the dielectric host.

The coordinates ξ_μ are succinctly defined in terms of the eccentricity of each surface. The eccentricity of the core-shell interface $e_c=(1-r_c^2)^{1/2}$ and the eccentricity of the shell-host interface $e_s=(1-r_s^2)^{1/2}$. For a prolate spheroid the coordinate in the coordinates are

$$\xi_\mu=1/e_\mu\ . \tag{3}$$

For the oblate spheroid the coordinate in the coordinates ξ_μ are imaginary and given by

$$\xi_\mu=[(1-e_\mu^2)/e_\mu^2]^{1/2}\ . \tag{4}$$

In the following development, the nonlinearity is restricted to the core region and is taken to be of the Kerr type. The dielectric function for the core material is thus

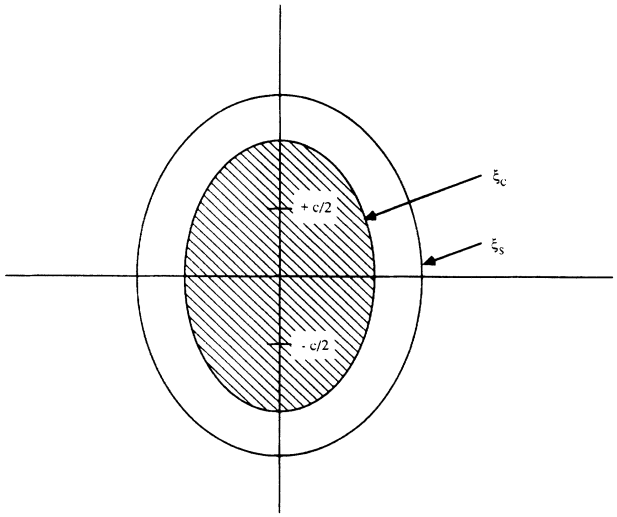

FIG. 1. Coated confocal spheroids. The core material is the nonlinear medium and the shell is metallic.

$$\epsilon_c=\epsilon_{\rm cl}+\chi_c^{(3)}|\mathbf{E}_L|^2\ . \tag{5}$$

The dielectric function $\epsilon_{\rm cl}$ is the complex linear part of the core dielectric function, $\chi_c^{(3)}$ is the complex Kerr coefficient for the core material, and $\mathbf{E}_L$ is the electric field in the core of the particle. Our Kerr-medium results are compared with specific models which include saturation in CuCl, CdS, and GaAs to show that our values are well within the limits imposed by the Kerr-medium approximation. The shell is metallic and has a complex dielectric coefficient ϵ_s, which is assumed independent of the field. The particles are embedded in a host dielectric material, which is assumed to be have a linear, lossless dielectric response ϵ_h.

Since the nonlinearity is restricted to the core region, we need only calculate the local field in the core to find the enhancement of the optical-nonlinear response. Since we assume that the particles are small compared to the wavelength [i.e. $(2\pi/\lambda)na_s\ll 1$, where n is the index of refraction of the metal], the quasistatic or Rayleigh approximation can be used. For the general case of the confocal spheroids (considering the z axis to be the direction of the symmetry axis of the particle) we obtain the expression for the local field in the core material:

$$E_L^m=\gamma_m E_0^m\ , \tag{6}$$

where $\mathbf{E}_0$ is the applied field in the host medium and γ_m is called the enhancement factor:

$$\gamma_m=\left[\frac{(1+A_s^m)(1+A_c^m)\epsilon_h\epsilon_s}{(\epsilon_c+A_c^m\epsilon_s)(\epsilon_s+A_s^m\epsilon_h)+\Gamma^m(\epsilon_c-\epsilon_s)(\epsilon_s-\epsilon_h)}\right]. \tag{7}$$

We label the nondegenerate axis with the superscript $m=0$ and the degenerate axes are labeled with the superscript $m=1$. The minor axes are degenerate in a prolate spheroid and the major axes are degenerate in an oblate spheroid. We note that the denominator of Eq. (7) is a quadratic function of $|\mathbf{E}_L|^2$, through the field dependence of ϵ_c given in Eq. (5). Therefore the relationship between the local-field amplitude and the applied-field amplitude is a cubic equation. The constants A_c^m are shape factors for the inner spheroid. A_s^m are shape factors for the outer spheroid. Γ^j are the shape factors which depend on the volume fraction of the shell. For the prolate spheroids the constants are ($\mu=c$ or s)

$$A_\mu^m=-\frac{P_1^m(\xi_\mu)}{Q_1^m(\xi_\mu)}\frac{Q_1^{m'}(\xi_\mu)}{P_1^{m'}(\xi_\mu)}\ . \tag{8}$$

The functions $P_n^m(x)$ and $Q_n^m(x)$ are the associated Legendre functions of first and second kind. The primes denote derivatives of these functions with respect to the argument. For oblate spheroids, substitute $i\xi_\mu$ for ξ_μ in the arguments of the functions. We shall use the convention in this paper of quoting results for the prolate spheroids and the oblate spheroid results are obtained by substitution of $i\xi$ and ξ in the arguments of the special

functions. The functions Γ^m introduced in the right-hand side of Eq. (7) are given by

$$\Gamma^m = -\frac{P_1^m(\xi_c)}{Q^m(\xi_c)}\frac{Q_1^{m'}(\xi_s)}{P_1^{m'}(\xi_s)} . \tag{9}$$

In the case of the coated sphere (i.e., in the limit $e_\mu \ll 1$) the shape coefficients reduce to

$$A_\mu^m = 2 ,$$
$$\Gamma^m = 2\left[\frac{a_s}{a_c}\right]^3 . \tag{10}$$

Substituting these values in Eq. (6), the solution for the local field of coated spheres is independent of the direction of the applied field and we drop the superscript m; the expression is

$$\mathbf{E}_L = \frac{9\epsilon_h\epsilon_s}{(\epsilon_c+2\epsilon_s)(\epsilon_s+2\epsilon_h)+2(a_c/a_s)^3(\epsilon_c-\epsilon_s)(\epsilon_s-\epsilon_h)}\mathbf{E}_0 . \tag{11}$$

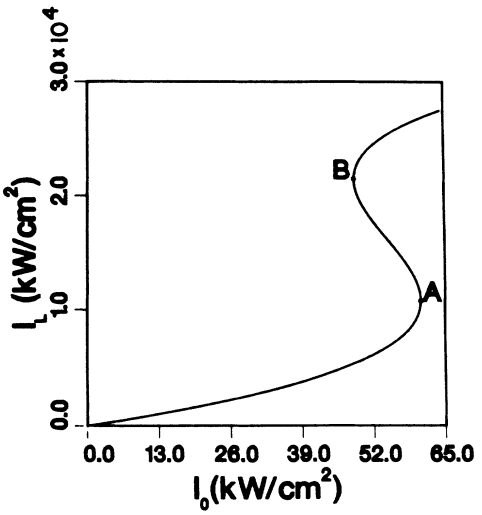

FIG. 2. Applied-field intensity vs local-field intensity for oblate spheroids with a silver shell and CuCl core. Field applied parallel to the symmetry axis.

We return now to the general relationship between the applied field and the local field inside the particle given by Eq. (6). We introduce two new scaled variables x and y. The square of the amplitude of the fields is denoted as

$$x = |E_L^m|^2$$

and

$$y = |9\epsilon_s\epsilon_h E_0^m|^2 . \tag{12}$$

The modulus squared of Eq. (6) is succinctly expressed when we introduce the notation

$$D = D_0 + D_1|E_L|^2 \tag{13}$$

for the denominator of the enhancement factor in Eq. (7). Equation (6) is transformed into the cubic equation

$$|D_1|^2x^3 + 2\,\mathrm{Re}(D_0D_1^*)x^2 + |D_0|^2x - y = 0 . \tag{14}$$

Re( ) denotes the real part of the quantity in parentheses and the asterisk superscript is complex conjugation of the variable. When this equation has three real roots in x for one value of the applied field y, the medium exhibits a bistable response. Each particle exhibits an *intrinsic* bistable phenomenon because it does not depend on feedback from an external cavity. The condition for the existence of optical bistability in a single particle is

$$4\,\mathrm{Re}(D_0D_1^*)^2 \geq 3|D_0|^2|D_1|^2 . \tag{15}$$

In the rest of this paper we test for the existence of IOB for various shell and core materials and optimize the geometric shape and the volumes of the core and shell materials.

The local-field intensity versus the applied-field intensity is shown in Fig. 2. We have chosen CuCl for the core, and the laser operating wavelength of 386.72 nm, which is close to the biexciton resonance. The shell material is silver and the host material is silica glass. The data for the linear dielectric constant of silver were taken from Ref. 11 and we used data for silica glass from Phillip.[12] The nonlinear susceptibility $\chi_c^{(3)}$ was calculated from the exciton-biexciton model for CuCl;[13] the salient features of this model are presented in Sec. III. The threshold intensity is at point A in Fig. 2 and the local field jumps discontinuously to the upper branch when the applied field is increased; beyond this the applied intensity at point A is about 60.5 kw/cm^2 at a wavelength 386.72 nm. This represents a reduction of 10^3 over the threshold intensity of uncoated metallic spheroidal particles.[5] It would be of great interest to synthesize particles of a prescribed geometry to precisely engineer the nonlinear-optical response. Further results for other materials are given in Sec. III.

The foregoing results are made for one particular orientation of the spheroidal particles. If the individual particles are not perfectly aligned in the medium, then the threshold intensities will be different among the collection of particles. However, this dependence is relatively weak, as we now show.

According to Eq. (6), the components of the local field (E_L^0, E_L^1) have different enhancement factors γ_0 and γ_1. Let us assume that we are tuned near the surface-plasmon resonance for $m=0$, i.e., $|\gamma_0| \gg |\gamma_1|$. The magnitude of the local field is related to the enhancement factors and the applied field by

$$|\mathbf{E}_L|^2 = (|\gamma_0|^2\cos^2\theta + |\gamma_1|^2\sin^2\theta)|E_0|^2 , \tag{16}$$

where θ is the angle that $\mathbf{E}_0$ makes with the axis $m=0$. both γ_0 and γ_1 depend on $|\mathbf{E}_L|^2$ through ϵ_m. The second term has a small enhancement factor and for θ small, sin θ is also small. For instance, when $|\theta| = 0.3$, the second term in Eq. (16) is only a 10% contribution to the total expression without accounting for the dominance of the enhancement factor γ_0. In this example, the orientations

can differ by $\pm 20°$ without significantly changing the threshold intensities.

B. Effective-medium approximation

When the nonlinear particles are dispersed in a host dielectric, the optical properties of the composite material will be quite different from the homogeneous host material. Nevertheless, an effective dielectric function can be used to describe the average optical response of the heterogeneous medium.

Since, in our case, the volume fractions of the particles are very low ($f \sim 10^{-3}$–10^{-6}), a much simpler description will suffice. If each of the coated inclusions were treated as a dipole, their contributions were summed up, and net polarization found for the medium, one could determine the effective dielectric function. For a single particle, the dipole moment (see the Appendix) is

$$p^m = \frac{E_0^m \tau^m}{4\pi} \left[\frac{(\epsilon_s - \epsilon_h)(\epsilon_c + A_c^m \epsilon_s) + G^m(\epsilon_c - \epsilon_s)(\epsilon_h + A_s^m \epsilon_s)}{(\epsilon_c + A_c^m \epsilon_s)(\epsilon_s + A_s^m \epsilon_h) + \Gamma^m(\epsilon_c - \epsilon_s)(\epsilon_s - \epsilon_h)} \right] , \tag{17}$$

where the two new coefficients in the numerator are ($m = 0, 1$)

$$G^m = \frac{P_1^m(\xi_c) Q_1^m(\xi_s)}{Q_1^m(\xi_c) P_1^m(\xi_s)} , \tag{18a}$$

and for a prolate spheroid

$$\tau^m = (1 + \delta_{m,0}) \frac{P_1^m(\xi_s)}{Q_1^m(\xi_s)} \frac{V}{\xi_s(\xi_s^2 - 1)} , \tag{18b}$$

where $\delta_{m,0}$ is the Kronecker delta. We give the explicit result for the oblate spheroid:

$$\tau^m = (1 + \delta_{m,0}) \frac{P_1^m(i\xi_s)}{Q_1^m(i\xi_s)} \frac{V}{\xi_s(\xi_s^2 + 1)} ; \tag{18c}$$

V is the volume of the coated particle. The volume of the prolate spheroid is

$$V = \frac{4\pi}{3} \left[\frac{c}{2} \right]^3 \xi_s(\xi_s^2 - 1) , \tag{19a}$$

and the oblate spheroid's volume is defined by

$$V = \frac{4\pi}{3} \left[\frac{c}{2} \right]^3 \xi_s(\xi_s^2 + 1) . \tag{19b}$$

The density of particles in the medium is N; the polarization when the particles are oriented in the same direction is

$$P^m = N p^m , \tag{20}$$

where p^m is given by Eq. (17).

The displacement field is related to the electric field and the polarization by $\mathbf{D} = \epsilon_h \mathbf{E} + 4\pi \mathbf{P}$. The polarization is proportional to the volume fraction of the coated particles, which is denoted by $f = NV$. Since the average dielectric tensor is defined by $\mathbf{D} = \vec{\epsilon} \cdot \mathbf{E}$, we find that it is diagonal and its components are given by

$$\bar{\epsilon}_m \simeq \epsilon_h + \frac{f \tau^m \epsilon_h}{V} \left[\frac{(\epsilon_s - \epsilon_h)(\epsilon_c + A_c^m \epsilon_s) + G^m(\epsilon_c - \epsilon_s)(\epsilon_h + A_s^m \epsilon_s)}{(\epsilon_c + A_c^m \epsilon_s)(\epsilon_s + A_s^m \epsilon_h) + \Gamma^m(\epsilon_c - \epsilon_s)(\epsilon_s - \epsilon_h)} \right] . \tag{21}$$

We remind the reader that Eq. (21) assumed that the particles are oriented inside the medium, but otherwise they have random positions. From Eq. (21) we note that the material exhibits both a linear and a nonlinear birefringence.

C. Propagation

We start with the wave equation for plane waves propagating along the x axis. We have for $m = 0$ the z polarization, and for $m = 1$, the y polarization of the light

$$\frac{\partial^2 E_m}{\partial x^2} - \frac{1}{c^2} \frac{\partial^2 E_m}{\partial t^2} = \frac{4\pi}{c^2} \frac{\partial^2 P_m}{\partial t^2} . \tag{22}$$

The nonlinear response is contained in the effective dielectric function $\bar{\epsilon}_m$ of Sec. II B. We introduce the slowly varying envelope function $E_0(x,t)$, which is related to the electromagnetic field E_m by

$$E_m = E_0(x,t) e^{i(kx - \omega t)} , \tag{23}$$

where ω is the angular frequency of the laser light. In order to simplify the notation, we suppress the subscript m on E_0 and k. The wave number k depends on the polarization and is chosen as $k^2 = (\omega^2/c^2)\mathrm{Re}(\bar{\epsilon}_{1m})$, where $\bar{\epsilon}_{1m}$ is the *linear* portion of the effective dielectric function in Eq. (21). This choice of k leaves a first-order differential equation for the slowly varying amplitude

$$\frac{\partial E_0}{\partial x} + \frac{1}{v_g} \frac{\partial E_0}{\partial t} - \frac{i\omega}{2 v_g} \frac{[\bar{\epsilon}_m - \mathrm{Re}(\bar{\epsilon}_{1m})]}{\mathrm{Re}(\bar{\epsilon}_{1m})} E_0 = 0 . \tag{24}$$

The group velocity is $v_g = c^2 k / \omega \, \mathrm{Re}(\bar{\epsilon}_{1m})$. This equation

is the basis for our study of light propagation through the heterogeneous material.

III. RESULTS AND DISCUSSION

Using the results of Sec. II we have performed numerical calculations on four different core materials coated by silver and with the host medium silica. For single particles we first optimize the particle shape and coating thickness so as to obtain the lowest value for the critical intensity at a particular frequency. The final optimal shape depends on the driving frequency of the laser, and the threshold values are very sensitive to the detuning. The sensitivity is dependent on the width of the resonance in the core material. This sensitivity will be discussed below.

Once the lowest thresholds at the appropriate laser frequency are achieved, we determine the nonlinear change of the dielectric constant in the transition between the two branches of the local-field solutions. The core material chosen in Fig. 2, CuCl, was selected because of its wide band gap and large nonlinear response. Our values are taken from Haus and co-workers;[3] the exciton-biexciton model has provided a good description of the nonlinear response below 77 K.

The dielectric function in the steady-state regime is given by

$$\epsilon_c=\epsilon_\infty+\frac{4\pi g_1^2\Delta'}{\delta'\Delta'-g_2^2|E_L|^2}\ . \tag{25}$$

The complex detuning parameters for the exciton resonance are

$$\delta'=\omega_e-\omega-i\tilde{\gamma}_e\ , \tag{26a}$$

and for the biexciton resonance they are

$$\Delta'=\omega_b-2\omega-i\tilde{\gamma}_b\ . \tag{26b}$$

The numerical values of the coefficients are given in Table I. The Kerr coefficient is given by

$$\chi_c^{(3)}=\frac{4\pi g_1^2 g_2^2}{\delta'^2\Delta'}\ ; \tag{27}$$

we have checked the convergence of the Taylor series expansion in our numerical results.

For the results reported in this paper, the dispersive contributions to the detuning are $(\omega_e-\omega)/\gamma_e=-118$ and $(\omega_b-2\omega)/\gamma_b=-133.3$. This is far from either resonance and the $\chi_c^{(3)}$ is dispersive; the absorption contribution is less than 1% of the dispersive portion.

The change of the real and imaginary parts of the average dielectric function, Eq. (21), are plotted in Figs. 3(a) and 3(b). These changes are much smaller due to the small volume fraction of particles in the medium $f=10^{-4}$. In CuCl both the real and imaginary parts of $\bar{\epsilon}$ increase for the high local-field branch, i.e., after the applied-field intensity exceeds the value given at point A in Fig. 2. The increase in the imaginary part of $\bar{\epsilon}$ is directly related to an increase in the absorption of light in the composite medium, which will have a significant

TABLE I. Model parameters for CuCl.

ϵ_∞	5
$4\pi g_1^2$	27.5 meV
g_2^2	1.8×10^9 MJ meV^2/cm^3
ω_e	3202.7 meV
ω_b	6372.5 meV
$\tilde{\gamma}_e$	0.03 meV
$\tilde{\gamma}_b$	0.3 meV

effect on the propagating field in the CuCl-silver-silica–composite medium. The dielectric function has a second discontinuity as the applied-field intensity is decreased; at point B in Fig. 2 the local field intensity can no longer be sustained at a large value and it collapses to a much smaller value on the lower branch.

We numerically solve Eq. (24) using standard integration methods. The thickness of the medium is 5 μm. Figure 4 is a plot of the applied-field intensity inside the medium for four values of the input intensity. The intensity of the applied field is continuous; at small values of

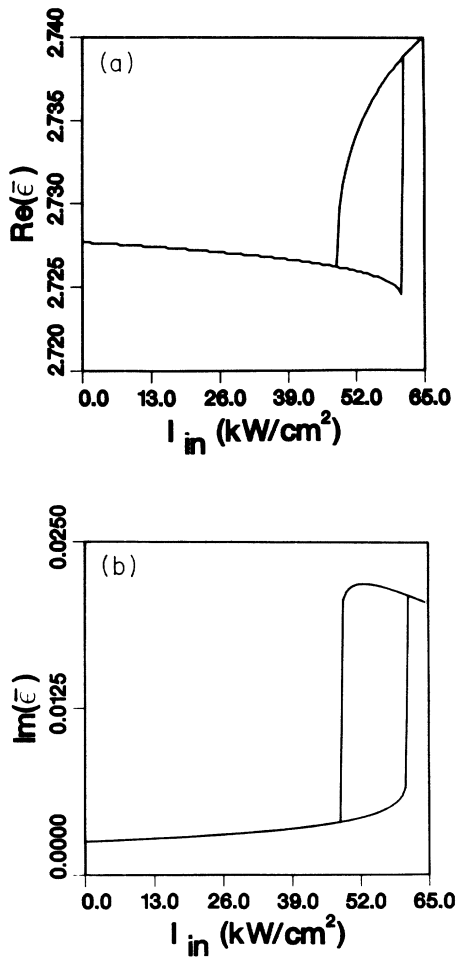

FIG. 3. (a) Real and (b) imaginary parts of the effective dielectric function for CuCl-Ag particles embedded in silica; $f=10^{-4}$.

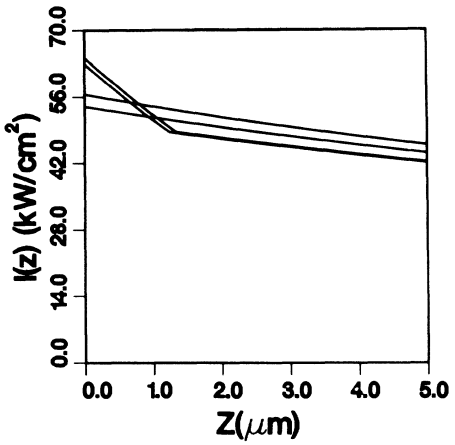

FIG. 4. Applied-field intensity vs depth in the medium for the same parameters used in Fig. 3.

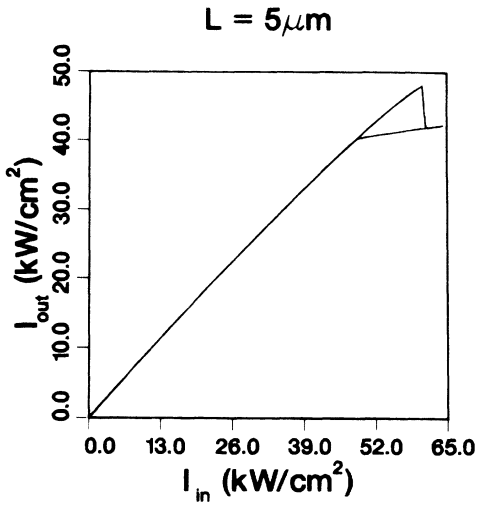

FIG. 6. Input intensity vs output intensity for CuCl-Ag particles in silica. Same parameters used in Fig. 3.

the input field (i.e., below the value at point A in Fig. 2), the field has a uniform change in its slope. When the applied field intensity is larger than the threshold value, the absorption is increased over a portion of the medium; then there is a discontinuous change in its slope as the high local-field collapses to a lower value. There is a boundary inside the medium characterized by the two branches of the local field, as shown in Fig. 5. This boundary has been discussed in the context of composite materials in an earlier publication.[8]

The output intensity versus input intensity is plotted in Fig. 6. The output decreases as the input intensity is ramped past the point A in Fig. 2. The high-absorption branch is flat because of the boundary between the high and low local fields inside the medium. As shown in Fig. 5, when the input intensity is increased, the output intensity varies only slightly. This is true as long as the boundary separating the high and low local-field values is inside the medium.

The high-absorption branch is a local effect and not due to any cavity feedback. Therefore the entire composite material returns to its original state when the intensity at the input face is below the value given by point B in Fig. 2.

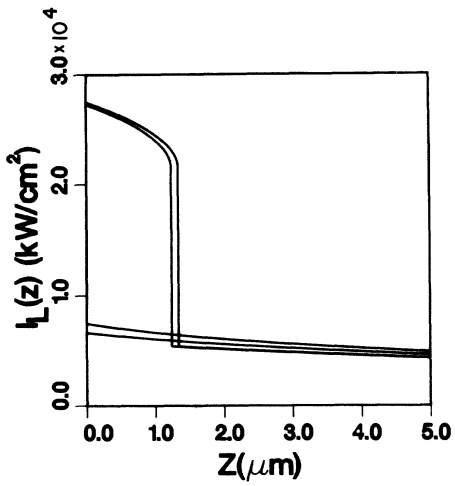

FIG. 5. Local-field intensity vs depth in the medium for the same parameters used in Fig. 3.

For the other materials reported below, we do not reproduce the propagation results. They will be qualitatively the same as the CuCl results presented above. All of our optimization parameters are reported for oblate spheroids with the field parallel to the symmetry axis. We have found similar optimized results for prolate spheroids, but the tendency of these crystallites is to grow as platelets. Silver metallic coatings have given us results that were consistently better than gold; this is due to the small value of the imaginary part of the dielectric constant of silver. The quoted value for CuCl in Table IV is optimized to a lower threshold compared to the value in Fig. 2 by changing the laser detuning to 386.7 nm. Note that this corresponds to a change of about 1 part in 10^5; thus the bistability is sensitive to changes of the laser frequency on this order of magnitude.

Two other semiconductors are of interest as candidate materials for intrinsic optical bistability: GaAs and CdS. CdS has a large band gap, and therefore its nonlinearity is resonant in a region where silver has a small imaginary component in the complex dielectric constant. We use the bound exciton resonance in CdS, which is a prominent feature in the absorption spectrum around 7 K.[14] We use a two-level model that has been fit to the experimental data. The small imaginary contribution to silver's dielectric constant will sharpen the surface-plasmon reso-

TABLE II. Model parameters for CdS.

ϵ_∞	6
β	40
$\tilde{\gamma}_x$	0.015 meV
ω_x	2555 meV
I_s	58 W/cm^2

TABLE III. Model parameters for GaAs.

ϵ_∞	12.6
β	48.8
$\tilde{\gamma}_x$	0.1 meV
ω_x	1515.5 meV
I_s	150 kW/cm^2

nance and help lower the threshold. GaAs has a band gap in the infrared, and the silver dielectric constant is broadened at these frequencies; a two-level model applied to the material at 77 K as well.[15] The values of $\chi^{(3)}$ are also complex for these materials and their values are determined from a two-level atomic model taken from the literature.[14,15]

The dielectric function for the two-level atomic model is

$$\epsilon_c=\epsilon_\infty+\frac{\beta(\delta+i)}{\delta^2+1+|E_L|^2/|E_s|^2}\ , \tag{28a}$$

where δ is the detuning of the laser from the exciton resonance and is given by

$$\delta=\frac{\omega_x-\omega}{\tilde{\gamma}_x}\ , \tag{28b}$$

where $\tilde{\gamma}_x$ is the resonance width for low intensities. The parameter $|E_s|^2$ is the saturation field for the excitation. In Tables II and III we quote the equivalent intensities $I_0=(cn/8\pi)|E_0|^2$. The parameters for CdS and GaAs are found in Tables II and III. The Kerr coefficient for the two-level model is

$$\chi_c^{(3)}=\frac{-\beta(\delta+i)}{(\delta^2+1)^2|E_s|^2}\ ; \tag{29}$$

in our studies the maximum value of the Taylor-series expansion parameter is 0.1. For CdS we chose the ratio of detuning to resonance width as $\delta=4.75$ and for GaAs it is $\delta=3.79$. In these materials we are tuned below the resonance.

Table IV summarizes our results for the three semiconductors discussed above. The laser wavelength and geometric factors are reported along with the expected switching intensity and the change of the semiconductor's refractive index. The changes are small and they are consistent with the Kerr approximation we made in the numerical results. The conversion between energy in eV and wavelength in nm is sensitive to the conversion factor. We use the relation $E(\text{eV})=1239.854/\lambda(\text{nm})$.

A fourth entry in Table IV includes the polymer core polydiacetylene (PDA). The advantage of PDA is its small linear dielectric constant $\epsilon=2.2$ and low absorption. The aspect ratio was made smaller than the other materials. We found a small change of the refractive index. The Kerr coefficient is $\chi_c^{(3)}=10^{-9}$ esu for PDA, which is much smaller than the value used for the semiconductors. The switching intensity is still reasonably small at 4.3 MW/cm,^{2} but not as low as the semiconductor core materials, which have much larger values for $\chi_c^{(3)}$.

IV. CONCLUSIONS

We have presented results on a composite material consisting of metal-coated particles with a nonlinear core. We have optimized the particle shape and coating thickness to obtain low thresholds for a set of four core materials. In this paper we reported results on oblate spheroids, although similar results were obtained with prolate spheroids.

The results presented in Sec. III (see also Table IV) show that the CdS core is by far the best material for further study. We have found a switching threshold of 12 W/cm.^{2} This represents a reduction of over six orders of magnitude from our previous results with silver particles alone.

In the event that the optimum shape and coating thickness cannot be fabricated, we still expect that very low thresholds can be achieved using these materials. Our intensities are within the limits of validity of the Kerr approximation and the changes of the refractive index are small.

The materials also have the advantage of a relatively low-absorption coefficient,[9] so that the particles can be packed to a high density in the host medium. At high densities, dipole-dipole interactions become important; this problem is currently being investigated.

As candidate materials to exhibit the intrinsic bistable effect, we propose that the material CdS be investigated further; it has an extremely low switching intensity. The technology for fabricating these particles in nanometer sizes is already achieved; new techniques need to be developed to coat the particles and engineer their shape. It is important to have precise control over the particle shapes; small variations will significantly shift the resonant frequency. The threshold intensities of these materi-

TABLE IV. Parameters for selected materials.

Material	Geometry a_c/a_s	Geometry r_c	λ (nm)	Switching intensity kW/cm^2	Δn
CuCl (oblate)	0.922	0.678	386.7	37.1	−0.143
CdS (oblate)	0.128	0.762	485.35	0.012	−0.352
GaAs (oblate)	0.892	0.436	818.32	29.3	−0.01
Polydiacetylene (oblate)	0.922	0.361	810.45	4.33×10^3	0.0002

als are well below the saturation values. The switching times of CuCl will be subnanosecond; this combined with the low-threshold intensity makes this material particularly promising for further investigations and possible device applications. We are optimistic that this new class of materials will provide real progress toward photonic materials that have potential device applications.

ACKNOWLEDGMENTS

This research was supported by National Science Foundation Grants No. ECS-8813028 and No. EET-8815141 and U.S. Defense Advanced Research Projects Agency Contract No. F19628-89-K-0045.

APPENDIX

The single-particle geometry is determined by the eccentricities of the core and shell, and the thickness of the metallic coat. In addition, we impose the constraint that the outer surface of shell be confocal with the surface of the core. If the foci of the spheroid are at $\pm c/2$ then

$$(a_c^2-b_c^2)^{1/2}=\frac{c}{2}=(a_s^2-b_s^2)^{1/2} , \tag{A1}$$

$$a_c[1-(b_c/a_c)^2]^{1/2}=a_s[1-(b_s/a_s)^2]^{1/2} , \tag{A2}$$

$$a_c e_c=a_s e_s . \tag{A3}$$

This reduces the number of independent parameters to two. We pick these to be the aspect ratio of the core (which defines e_c), and the ratio of the core and shell major axes.

To solve for the local field in the core of the particle, it is convenient to work with the appropriate spheroidal coordinates system (ξ,η,φ).[16] In this system, surfaces of constant ξ are spheroids, those of constant η are hyperboloids of two sheets, and those of constant φ are planes containing the $\hat{\mathbf{e}}_z$ axis.

We take the spheroid with its symmetry axis along the $\hat{\mathbf{e}}_z$ direction, the incident field $\mathbf{E}_0=E_0-\hat{\mathbf{e}}_z$ for $m=0$, and $\mathbf{E}_0=E_0\hat{e}_y$ for $m=1$. Since we are in the quasistatic region ($\lambda \ll a_s$), we only need to solve Laplace's equation, the general solution to which can be written

$$\psi=\sum_{l,m} A_{l,m}[P_l^m(\xi)+B_{l,m}Q_l^m(\xi)]P_l^m(\eta)e^{im\varphi} . \tag{A4}$$

This expansion is used to write the potential for the three regions: the core, the shell, and the host material external to the particle. For very large distances from the particle the potential is

$$\psi_e^m=\begin{cases} -E_0 z & \text{for } m=0 \\ -E_0 y & \text{for } m=1 , \end{cases} \tag{A5}$$

which in prolate spheroidal coordinates is

$$\psi_e^m=\begin{cases} -\frac{c}{2}E_0\xi\eta & \text{for } m=0 \\ -\frac{c}{2}E_0(\xi^2-1)^{1/2}(1-\eta^2)^{1/2}\sin\varphi & \text{for } m=1 , \end{cases} \tag{A6}$$

which reduces Eq. (A4) to

$$\psi^m=-\frac{c}{2}E_0[P_1^m(\xi)+BQ_1^m(\xi)]P_1^m(\eta)e^{im\varphi} . \tag{A7}$$

The boundary conditions can now be applied to Eq. (A7). Across each interface, we require (a) the potential to be continuous and (b) the normal component of $\mathbf{D}$ to be continuous:

$$\begin{aligned} &\psi_e^m(\xi=\xi_s)=\psi_s^m(\xi=\xi_s) , \\ &\psi_s^m(\xi=\xi_c)=\psi_c^m(\xi=\xi_c) , \\ &\epsilon_h\left[\frac{\partial\psi_e^m}{\partial\xi}\right]_{\xi=\xi_s}=\epsilon_s\left[\frac{\partial\psi_s^m}{\partial\xi}\right]_{\xi=\xi_s} , \\ &\epsilon_s\left[\frac{\partial\psi_s^m}{\partial\xi}\right]_{\xi=\xi_c}=\epsilon_c\left[\frac{\partial\psi_c^m}{\partial\xi}\right]_{\xi=\xi_c} . \end{aligned} \tag{A8}$$

Note the ψ_c^m will not have a term in $Q_1^m(\xi)$ as this is divergent at $\xi=1$. Solving Eq. (A8) for the potential in the core,

$$\psi_c^m=B_c^m P_1^m(\xi)P_1^m(\eta) . \tag{A9}$$

Defining A_c^m, A_s^m, and Γ^m as in Eqs. (6) and (7), and solving Eqs. (A8), we find the local field in the core to be

$$E_L^m=\gamma_m E_0^m , \tag{A10}$$

where γ_m is given by Eq. (7). Next, to find the dipole moment of the single particle, we look at the potential outside the particle:

$$\psi_e^m=-\frac{c}{2}E_0[P_1^m(\xi)+B_e Q_1^m(\xi)]P_1^m(\eta) . \tag{A11}$$

The first term is the potential due to the external field. The second term in the expression [i.e., the term in $Q_1^m(\xi)$] is the potential due to a dipole. Hence its coefficient $-(c/2)E_0B_e$ is related to the induced dipole moment of a particle. The second term decays asymptotically as $1/r^2$; the coefficient is related to the dipole moment, which is given in Eq. (17).

[1]L. K. H. Van Beek, in *Progress in Dielectrics*, edited by J. B. Birks (CRC, Cleveland, 1967), Vol. 7, p. 69.

[2]R. K. Jain and R. C. Lind, J. Opt. Soc. Am. **73**, 647 (1983).

[3]P. Roussignol, D. Ricard, J. Lukasik, and C. Flytzanis, J. Opt. Soc. Am. B **4**, 5 (1987).

[4]D. Ricard, P. Roussignol, and C. Flytzanis, Opt. Lett. **10**, 511 (1985); F. Hache, D. Ricard, and C. Flytzanis, J. Opt. Soc. Am. B **3**, 1647 (1986); F. Hache, D. Ricard, C. Flytzanis, and U. Kreibig, Appl. Phys. A **47**, 347 (1988).

[5]J. W. Haus, N. Kalyaniwalla, R. Inguva, M. Bloemer, and C.

M. Bowden, J. Opt. Soc. Am. B **6**, 797 (1989); J. W. Haus, R. Inguva, and C. M. Bowden, Phys. Rev. A **40**, 5729 (1989).

[6]M. J. Bloemer, J. W. Haus, and P. R. Ashley J. Opt. Soc. Am. B **7**, 790 (1990); M. J. Bloemer, P. R. Ashley, J. W. Haus, N. Kalyaniwalla, and C. R. Christensen, IEEE J. Quantum. Electron. **26**, 1075 (1990).

[7]Al. L. Efros and A. L. Efros, Fiz. Tekh. Poluprovdn. **16**, 1209 (1982) [Sov. Phys.—Semicond. **16**, 772 (1982); A. I. Ekimov and A. A. Onushchenko, Fiz. Tekh. Poluprovdn. **16**, 1215 (1982); [Sov. Phys.—Semicond. **16**, 775 (1982)]; A. I. Ekimov, Al. L. Efros, and A. A. Onushchenko, Solid State Commun. **56**, 921 (1985); E. Hanamura, Phys. Rev. B **37**, 1273 (1988).

[8]J. W. Haus, N. Kalyaniwalla, R. Inguva, and C. M. Bowden, J. Appl. Phys. **65**, 1420 (1989).

[9]A. E. Neeves and M. H. Birnboim, J. Opt. Soc. Am. B **6**, 787 (1989); Opt. Lett. **13**, 1087 (1988). For coated sphere solutions, see also C. F. Bohren and D. R. Huffman, *Absorption and Scattering of Light by Small Particles* (Wiley, New York, 1983). Multiply coated spheres were investigated in M. H. Birnboim and W. P. Ma, Mater. Res. Soc. Symp. Proc. **164**, 277 (1990).

[10]Results were also reported at conferences: M. H. Birnboim, J. W. Haus, N. Kalyaniwalla, W. P. Ma, and R. Inguva, Opt. News **15**, A81 (1989); N. Kalyaniwalla, J. W. Haus, M. H. Birnboim, W. P. Ma, and R. Inguva, Mater. Res. Soc. Symp. Proc. **164**, 283 (1990); M. H. Birnboim, W. P. Ma, J. W. Haus, N. Kalyaniwalla, and R. Inguva, SPIE Proc. (to be published).

[11]*Handbook of Optical Constants of Solids,* edited by E. D. Palik (Academic, New York, 1985).

[12]H. R. Phillip, J. Phys. Chem. Solids **32**, 1935 (1971).

[13]J. W. Haus, C. M. Bowden, and C. C. Sung, Phys. Rev. A **31**, 1936 (1985); C. C. Sung, C. M. Bowden, J. W. Haus, and W. K. Chiu, *ibid.* **30**, 1873 (1984).

[14]M. Dagenais, Appl. Phys. Lett. **43**, 742 (1983).

[15]D. S. Chemla, D. A. B. Miller, P. W. Smith, A. C. Gossard, and W. Wiegmann, IEEE J. Quantum Electron. **QE-20**, 2655 (1986); D. S. Sell, S. E. Stokowski, R. Dingle, and J. V. DiLorenzo, Phys. Rev. B **7**, 4568 (1973).

[16]P. M. Morse and H. Feshbach, *Methods of Theoretical Physics* (McGraw-Hill, New York, 1953), Vol. 2.